JCAMECH

Transverse sensing of simply supported truncated conical shells

Rasa Jamshidi [a]∗, Ali Asghar Jafari [a,]

[a] Khaje Nasir University of Technology, Mechanical Engineering Department, Tehran, Iran

---

ARTICLE INFO

ABSTRACT

Modal signals of transverse sensing of truncated conical shells with simply supported boundary condition at both ends are investigated. The embedded piezoelectric layer on the surface of conical shell is used as sensors and output voltages of them in considered modes are calculated. The Governing sensing signal displacement equations are derived based on the Kirchhoff theory, thin-shell assumption, piezoelectric direct effect, the Gauss theory and the open circuit assumption. A conical shell with fully covered piezoelectric layer is considered as a case study and the layer is segmented into 400 patches. Modal voltages of the considered model are calculated and evaluated. The ideal locations for sensor patches are in the middle of conical shell surface in the longitudinal direction and locations near the ends of the conical shell are not recommended. The longitudinal membrane strain signal has a leading role on the total signal in comparison with other strain signal components. The output signals of the sensor can be used as a controller input for later active vibration control or structural health monitoring.

---

1. Introduction

Thin walled conical structures are widely used in various industries like aerospace, offshore, civil and other fields of engineering. For example, in the pressure hulls of submarines conical shells are used frequently. In turbojet engines conical shells are used in exhaust nozzle. Different kinds of environmental conditions may cause these structures to encounter undesirable vibrations. Therefore, the dynamic and characteristics of these structures are important and should be investigated carefully. Precise measurement of the conical shell vibration has a leading role in smart structures, active vibration control and structural health monitoring. There are many ways to measure the vibration of conical shells. Most of them have a weakness in which the added mass of the sensor to the structure causes the measurement, imprecise. After invention of the smart materials, tendencies for smart structures have been increased and these materials can be used as a sensor. One of the ways to overcome the sensor mass add on effect is the distributed sensing method with piezoelectric layer. Piezoelectric materials have a lightweight and less power consumption and energy conversion which solves the sensor mass add on problem [1]. Because of the piezoelectric lightweight feature, it is applicable in the aerospace industries.

The signals of the piezoelectric layer sensor are functions of the conical shell strains and it can show the structure's deformation shape. These sensors are useful in smart structures

for many types of applications, e.g., vibration isolation, vibration control, structural health monitoring, etc. In piezoelectric sensors, the direct effect of piezoelectric layer is used. In this condition, a displacement or strain is imported into the piezoelectric layer and the piezoelectric layer converts the displacement into the voltage signal. The sensor output voltage distribution shows the shell surface displacement.

If a sensor cannot observe the shell vibration correctly, the smart structure cannot comply the designed intended purpose of the structure. For example, in active vibration control application, if the sensor observability diminishes, then the smart structure could not compensate the vibrations and even it may cause the vibrations to magnify. In the structure distributed sensing, sensor segmentation is very important and as the segmentation increases the observability of the distributed sensors increases.

The piezoelectric sensor can sense bending, membrane and torsional strains. The boundary condition of the conical shell which is considered in this investigation is simply supported at both ends. Since in simply supported boundary condition, the conical shell cannot tolerate torsional vibrations, only transverse vibration sensing (membrane and bending strains sensing) are described here.

So far, numerous studies have been carried out concerning the vibration characteristic of conical shells. But researches about modal sensing of conical shells are not numerous and the literature is scarce. Li et al [2] calculated natural frequency and

---

∗ Corresponding author. e-mail: rs.jamshidi@mail.kntu.ac.ir

forced vibration response of conical shells with Rayleigh–Ritz method. This method is a good approach and its accuracy is acceptable. Vibration analysis of rotating simply supported truncated circular conical shells was studied by Lam and Hua [3]. The mode shape function, which was used, was simple and applicable with an acceptable error. Torsion and transverse sensing of clamped-free conical shells was studied by Li et al [4]. Modal signals of transverse sensing were derived and explained in the clamped-free boundary condition. Tzou et al [5] investigated the distributed sensing characteristics of conical shells, and showed that the sensing signals of each mode consisted of four components, related to the four strain items, i.e., the longitudinal membrane, the circumferential membrane, the longitudinal bending and the circumferential bending strain. Neural potentials and micro-signals of non-linear deep and shallow conical shells are studied by Chai et al [6]. Free-free boundary condition in the conical shell was considered and the results showed that in this boundary condition, the dominating signal component among four contributing micro-signal components was the circumferential membrane component. Li et al [7] studied active vibration control of conical shells using piezoelectric materials. Velocity feedback control method was applied to control the undesired vibrations. Actuator were only distributed circumferentially and the sensor distribution was not considered.

Mechanical behaviors of the Nano structures like nanorods, nanobeams and nanoplates have attracted many researchers' attention. The dynamic of these structures is very important and the nonlocal theory is used to analysis the characteristics of them. Dynamics and characteristics of nanorods and nanobeams were discussed by many researchers. Surface energy effect on the rotating nanobeam vibration analysis was studied by Safarabadi et al [8]. Mohammadi et al evaluated hygro-mechanical vibration analysis of a rotating viscoelastic nanobeam [9]. Axial vibration analysis of a tapered nanorod was studied by Danesh et al [10]. Nanoplates have many applications in different kinds of industries and this phenomenon cause the researchers to investigate in this field. Thermo-mechanical vibration analysis of circular and annular nanoplate were studied by Goodarzi et al [11]. Free vibration analysis of sector plate was studied by Mohammadi et al [12] and a new version of differential quadrature method was used. Vibration frequency analysis of rectangular nanoplate was discussed by Goodarzi et al [13]. Vibration analysis of piezoelectric nanofilm-based electromechanical sensors was evaluated by Farajpour et al [14]. Small scale effect on the vibration of orthotropic plates was studied by Mohammadi et al [15]. Nanoscale mass detection based on the vibrating piezoelectric ultrathin film was investigated by Asemi et al [16]. Farajpour et al studied buckling analysis of nanoplates [17-25]. Influence of initial stress on the vibration of double-piezoelectric-nanoplate systems were studied by Asemi et al [26]. Nonlocal nonlinear plate model for large amplitude vibration of magneto-electro-elastic nanoplates were studied by Farajpour et al [27]. A study on the nonlinear stability of orthotropic single-layered graphene sheet based on the nonlocal elasticity theory was investigated by Asemi et al [28]. Mohammadi et al studied various conditions effects on the graphene sheet vibration and buckling [17-25]. Vibration, buckling and smart control of microtubules using piezoelectric nanoshells were studied by Farajpour et al [29, 30]. Nonlinear vibration analysis of piezoelectric nanoelectromechanical resonators based on the nonlocal elasticity theory was studied by Asemi et al [31]. Vibration analysis of nanorings using nonlocal

continuum mechanics and shear deformable ring theory was studied by Moosavi et al [32].

In the past, only two types of boundary conditions (i.e. free-free and clamped-free) for modal sensing of truncated conical shells have been studied and other types of boundary conditions have not been investigated. Since the boundary condition has a significant effect on the dynamic and characteristics of the shell, a structure should be studied separately in each kind of boundary conditions.

Determining modal signals of the simply supported truncated conical shell with piezoelectric layer, which is used as sensors, is the focus of this study. For sensing the transverse vibrations, thin piezoelectric layer is laminated on the shell surface. Firstly, membrane and bending strains of thin conical shells are extracted based on the Kirchhoff theory. Then, transverse sensing of conical shells with piezoelectric layers is derived based on the piezoelectric direct effect and the Gauss theory. Due to the sensor output signal complexity, the modal signal is separated into four parts, which are defined as: the longitudinal membrane, the longitudinal bending, the circumferential membrane and the circumferential bending strain signal. Modal functions of simply supported conical shells are extracted for modal sensor signal calculations. For evaluating the sensor performance, a case study is considered. In this case piezoelectric layer covers the entire surface of the conical shell. Modal voltages of considered modes are calculated in each patch. The numerical results indicate the location of the total signal output maximum and minimum in considered mode shapes. This method leads to better positioning of the ideal locations for sensor patches. The proposed method is capable of determining the modal participation factors, while the testing signal is available. It is also capable of determining the mode shapes by using several distributed sensor segments.

2. Thin conical shell strain displacement relation

Conical shells constitute a special type of shells of revolution and can have either circular or elliptic cross sections. Only conical shells with circular cross sections are considered here. The corresponding curvilinear coordination $O_{x\theta z}$ and its origin are shown in the Figure.1. The conical shell is made of isotropic material.

In the coordination shown in the Figure.1, t, x and z represents the circumferential direction, the longitudinal direction and the transverse direction, respectively. The fundamental form of shells for curvilinear coordinate in the conical shell can be written as:

$$ds^2 = dx^2 + x\sin(c)dt^2 \qquad (1)$$

Where c is the conic angle (Figure.1). Lame parameters and radii of curvatures in conical shells can be extracted from Eq. (1).

$$A_x = 1 \qquad (2.a)$$

$$A_t = x\sin(c) \qquad (2.b)$$

$$R_x = \infty \qquad (2.c)$$

$$R_t = x\tan(c) \qquad (2.d)$$

Strain-displacement relations for thin conical shell based on the Kirchhoff-Love theory and linear variations of in-plane displacements are derived. Strain expressions S_{ij} are separated into two parts, which are named as: the membrane strains (S_{ij}^0) and the bending strains (k_{ij}).
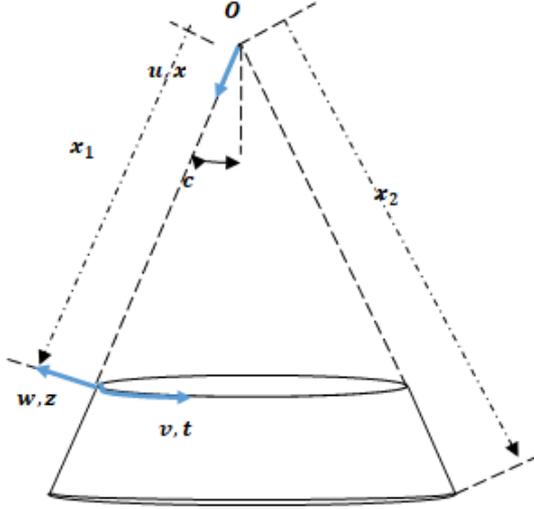
Figure 1. A truncated conical shell model

$$S_{xx} = S_{xx}^0 + zk_{xx} \qquad (3.a)$$

$$S_{tt} = S_{tt}^0 + zk_{tt} \qquad (3.b)$$

$$S_{xt} = S_{xt}^0 + zk_{xt} \qquad (3.c)$$

The membrane strains in thin conical shell are defined as:

$$S_{xx}^0 = \frac{\partial u}{\partial x} \qquad (4.a)$$

$$S_{tt}^0 = \frac{u}{x} + \frac{1}{xsin(c)}\frac{\partial v}{\partial t} + \frac{w}{xtan(c)} \qquad (4.b)$$

$$S_{xt}^0 = \frac{1}{xsin(c)}\frac{\partial u}{\partial t} - \frac{v}{x} + \frac{\partial v}{\partial x} \qquad (4.c)$$

Where u, v and w are the displacement in the longitudinal, the circumferential and the transverse direction, respectively. (Figure.1). Similarly, the bending strains in thin conical shell are defined as:

$$k_{xx} = -\frac{\partial^2 w}{\partial x^2} \qquad (5.a)$$

$$k_{tt} = \frac{cos(c)}{\left(xsin(c)\right)^2}\frac{\partial v}{\partial t} - \frac{1}{\left(xsin(c)\right)^2}\frac{\partial^2 w}{\partial t^2} - \frac{1}{x}\frac{\partial w}{\partial x} \qquad (5.b)$$

$$k_{xt} = \frac{1}{xtan(c)}\frac{\partial v}{\partial x} - \frac{2v}{x^2 \tan(c)} - \frac{2}{xsin(c)}\frac{\partial^2 w}{\partial x\partial t} + \frac{2}{x^2 \sin(c)}\frac{\partial w}{\partial t} \qquad (5.c)$$

The aforementioned strain displacements equations will be used for modal signal calculations, which will be described in the next section.

3. Transverse sensing of conical shells

Piezoelectric patches are polarized only in the transverse direction and it is used for sensing the transverse vibrations of conical shells. The sensor is sensitive to transverse modes and insensitive to in-plane shear strains. The conical shell sensing signal equation is derived based on the direct piezoelectric effect, the Gauss theory, the Maxwell equation and the open circuit assumption. Generally in conical shells, strains in the neural sensor layer contribute to the signal generation Q^s [5]:

$$Q^s = \frac{h^s}{S^e}\iint_{x\,t}\left(h_{31}S_{xx} + h_{32}S_{tt} + h_{36}S_{xt}\right)dS^e =$$

$$\frac{h^s}{S^e}\iint_{x\,t}\left(h_{31}S_{xx} + h_{32}S_{tt} + h_{36}S_{x\theta}\right)x\,sin(c)dtdx \qquad (6)$$

Where the superscript 's' denotes the distributed sensor layer. The parameters h^s and S^e are the thickness of the sensor layer and the effective electrode area of the sensor layer, respectively. h_{31}, h_{32} and h_{36} are the piezoelectric constants. The effect of transverse strains S_{xz}, $S_{\theta z}$ and S_{zz} are neglected, since the variation in the transverse direction is small and the shell and the sensor layer are thin. Moreover, the sensor material is assumed to be insensitive to the in plane twisting $S_{x\theta}$. Therefore, the Eq. (6) becomes

$$Q^s = \frac{h^s}{S^e}\iint_{x\,t}\left(h_{31}S_{xx} + h_{32}S_{tt}\right)x\,sin(c)dtdx =$$

$$\frac{h^s}{S^e}\iint_{x\,t}\left(h_{31}\left(S_{xx}^0 + zk_{xx}\right) + h_{32}\left(S_{tt}^0 + zk_{tt}\right)\right)x\,sin(c)dtdx \qquad (7)$$

The effective electrode area of the sensor layer is calculated by:

$$S^e = \iint_{x\,t}x\,sin(c)dtdx = \frac{1}{2}\left(x_2^{s2} - x_1^{s2}\right)\left(t_2^s - t_1^s\right)sin(c) \qquad (8)$$

where x_2^s and x_1^s are the intervals of the patch surface in the longitudinal direction and t_2^s and t_1^s are the intervals of the patch surface in the circumferential direction. Considering the Eq.4, 5, the Eq.7 can be written as:

$$Q^s = \frac{h^s}{S^e}\iint\limits_{x\,t}\left[\begin{array}{l} h_{31}\left(\dfrac{\partial u}{\partial x}-z\dfrac{\partial^2 w}{\partial x^2}\right)+ \\[2mm] h_{32}\left(\begin{array}{l} \dfrac{u}{x}+\dfrac{1}{x\sin(c)}\dfrac{\partial v}{\partial t}+\dfrac{w}{x\tan(c)}+ \\[2mm] z\left(\begin{array}{l} \dfrac{\cos(c)}{(x\sin(c))^2}\dfrac{\partial v}{\partial t} \\[2mm] -\dfrac{1}{x\sin(c)}\dfrac{\partial^2 w}{\partial t^2} \end{array}\right) \\[2mm] -\dfrac{1}{x}\dfrac{\partial w}{\partial x} \end{array}\right) \end{array}\right] x\sin(c)\,dtdx$$

$$(9)$$

The Eq.9 describes the total output signal of a sensor, which is caused by the membrane and bending strains. The developed equation is very complex. Owing to the complexity of this equation, the sensor total signal is separated into four parts. These four parts are defined as: the longitudinal membrane strain signal ($Q^s_{S^0_{xx}}$), the longitudinal bending strain signal ($Q^s_{k_x}$), the circumferential membrane strain signal ($Q^s_{S^0_{tt}}$) and the circumferential bending strain signal ($Q^s_{k_t}$). The total sensor voltage can be written as [4]:

$$Q^s = Q^s_{S^0_{xx}} + Q^s_{k_x} + Q^s_{S^0_{tt}} + Q^s_{k_t} \qquad (10)$$

Where, each part is described by:

$$Q^s_{S^0_{xx}} = \frac{h^s}{S^e}\iint\limits_{x\,t}\left(h_{31}\frac{\partial u}{\partial x}\right)x\,\sin(c)\,dtdx \qquad (11.\text{a})$$

$$Q^s_{k_x} = -\frac{h^s}{S^e}\iint\limits_{x\,t}\left(h_{31}z\frac{\partial^2 w}{\partial x^2}\right)x\,\sin(c)\,dtdx \qquad (11.\text{b})$$

$$Q^s_{S^0_{tt}} = \frac{h^s}{S^e}\iint\limits_{x\,t}\left(h_{32}\left(\frac{u}{x}+\frac{1}{x\sin(c)}\frac{\partial v}{\partial t}+\frac{w}{x\tan(c)}\right)\right)x\,\sin(c)\,dtdx \qquad (11.\text{c})$$

$$Q^s_{k_t} = \frac{h^s}{S^e}\iint\limits_{x\,t}\left[h_{32}z\left(\begin{array}{l} \dfrac{\cos(c)}{(x\sin(c))^2}\dfrac{\partial v}{\partial t} \\[2mm] -\dfrac{1}{(x\sin(c))^2}\dfrac{\partial^2 w}{\partial t^2} \\[2mm] -\dfrac{1}{x}\dfrac{\partial w}{\partial x} \end{array}\right)\right] x\,\sin(c)\,dtdx \qquad (11.\text{d})$$

The sensor total signal (Eq.9) and its components (Eq.11) in the conical shell are defined. For calculating modal voltage of each component, modal displacement function should be derived. In the next section modal displacement functions for simply supported truncated conical shells are described.

4. Modal Displacement Functions

In this section modal displacement function of the conical shell is derived. The boundary condition of truncated conical shell is assumed to be simply support at both ends. The proposed modal displacement function should satisfy the geometric and the force boundary conditions in the simply supported condition. The principal mode shapes of the conical shells with two simply supported boundaries can be expressed as [6]:

$$U(x,t)=\sum_{m=1}^{\infty}\sum_{n=1}^{\infty}\cos\left(\frac{m\pi(x-x_1)}{x_2-x_1}\right)\cos(nt)\eta_{xmn} \qquad (12.\text{a})$$

$$V(x,t)=\sum_{m=1}^{\infty}\sum_{n=1}^{\infty}\sin\left(\frac{m\pi(x-x_1)}{x_2-x_1}\right)\sin(nt)\eta_{\theta mn} \qquad (12.\text{b})$$

$$W(x,t)=\sum_{m=1}^{\infty}\sum_{n=1}^{\infty}\sin\left(\frac{m\pi(x-x_1)}{x_2-x_1}\right)\cos(nt)\eta_{zmn} \qquad (12.\text{c})$$

where m and n are the wave numbers in the longitudinal and circumferential directions, respectively. It should be noted that the Eq.12 satisfies the geometric boundary conditions accurately, but some of the force boundary conditions are not satisfied for the simply supported boundary conditions [2]. However, the mode shapes given by the Eq.12 are simple in the form and previous studies has shown that these errors are acceptable in small deformations, especially when the conical shell is not subjected to forces along the longitudinal direction. On the other hand, for such complicated strain equations as discussed in this paper, the modal displacement function is obviously simpler and thus more applicable. Therefore, these mode shapes can be used in the simply supported boundary conditions [6]. So, from the Eq.12; mode shape of each displacement can be defined as:

$$u=\cos\left(\frac{m\pi(x-x_1)}{x_2-x_1}\right)\cos(nt) \qquad (13.\text{a})$$

$$v=\sin\left(\frac{m\pi(x-x_1)}{x_2-x_1}\right)\sin(nt) \qquad (13.\text{b})$$

$$w=\sin\left(\frac{m\pi(x-x_1)}{x_2-x_1}\right)\cos(nt) \qquad (13.\text{c})$$

Considering the proposed mode shapes, the four modal signal components can be expressed as:

$$Q^s_{S^0_{xx}} = -\frac{h^s h_{31}m\pi\sin(c)}{S^e(x_2-x_1)}\iint\limits_{x\,t}x\sin\left(\frac{m\pi(x-x_1)}{x_2-x_1}\right)\cos(nt)\,dtdx \quad (14.\text{a})$$

$$Q^s_{k_x} = \frac{h^s h_{31}r^s_x\sin(c)}{S^e}\left(\frac{m\pi}{x_2-x_1}\right)^2\iint\limits_{x\,t}x\sin\left(\frac{m\pi(x-x_1)}{x_2-x_1}\right)\cos(nt)\,dtdx \quad (14.\text{b})$$

$$Q_{S_{tt}^0}^s = \frac{h^s h_{32}}{S^e} \iint\limits_{x\,t} \left[\begin{array}{c} (n+\cos(c))\sin\left(\dfrac{m\pi(x-x_1)}{x_2-x_1}\right)+ \\ \sin(c)\cos\left(\dfrac{m\pi(x-x_1)}{x_2-x_1}\right) \end{array} \right] \cos(nt)\,dtdx \quad (14.c)$$

$$Q_{k_\theta}^s = \frac{h^s h_{32} r_t^s}{S^e} \iint\limits_{x\,t} \left[\begin{array}{c} \dfrac{n^2+ncos(c)}{xsin(c)}\sin\left(\dfrac{m\pi(x-x_1)}{x_2-x_1}\right) \\ -\dfrac{m\pi\sin(c)}{x_2-x_1}\cos\left(\dfrac{m\pi(x-x_1)}{x_2-x_1}\right) \end{array} \right] \cos(nt)\,dtdx \quad (14.d)$$

These four modal signal components can be calculated for any kind of sensor distribution in the surface of conical shell. If the piezoelectric layer covers the entire surface of the conical shell, the integral intervals in the longitudinal direction and circumferential direction will cover the entire conical shell surface. Various types of sensor distribution change the integral intervals of each component and this alters the total sensor signal. To generalize the results, it is considered that the entire conical shell surface is fully covered with piezoelectric sensors and in this case the signals of each component in considered modes are calculated. The major limitation of the suggested methodology is that forces in the longitudinal direction can cause the modal displacement functions become unreliable and this causes the modal displacement faulty.

5. Point sensing signals

The sensor output voltage signal (Eq.6) represents the sensing signal of piezoelectric patch or a piezoelectric stripe, which is laminated on the conical shell. This equation represents an average voltage over the sensor patch area. This area can be reduced to an infinitesimally small area. This phenomenon causes the average to be neglected and the signal becomes the point-sensing signal at the sensor location. The global distributions of these signals over the surface of the shell reveal the conical shell mode shape, i.e., the modal signals. In this case the sensing signal becomes [4]:

$$Q^s(x,t) = h^s \left(h_{31}S_{xx} + h_{32}S_{tt} \right) \quad (15)$$

Considering the Eq.3, the sensing signal becomes

$$Q^s(x,t) = h^s h_{31}S_{xx}^0 + h^s h_{31}r_x^s k_x + h^s h_{32}S_{tt}^0 + h^s h_{32}r_t^s k_t \quad (16)$$

The point sensing signal can be separated into four components,

$$Q_{S_{xx}^0}^s(x,t) = h^s h_{31}S_{xx}^0 =$$
$$-\frac{h^s h_{31}m\pi}{x_2-x_1}\sin\left(\frac{m\pi(x-x_1)}{x_2-x_1}\right)\cos(nt) \quad (17.a)$$

$$Q_{k_x}^s(x,t) = h^s h_{31}r_x^s k_x =$$
$$h^s h_{31}r_x^s\left(\frac{m\pi}{x_2-x_1}\right)^2\sin\left(\frac{m\pi(x-x_1)}{x_2-x_1}\right)\cos(nt) \quad (17.b)$$

$$Q_{S_{\theta\theta}^0}^s(x,t) = h^s h_{32}S_{tt}^0 =$$
$$h^s h_{32}\left[\begin{array}{c} \dfrac{1}{x}\cos\left(\dfrac{m\pi(x-x_1)}{x_2-x_1}\right)+ \\ \dfrac{n+\cos(c)}{xsin(c)}\sin\left(\dfrac{m\pi(x-x_1)}{x_2-x_1}\right) \end{array} \right]\cos(nt) \quad (17.c)$$

$$Q_{k_t}^s(x,t) = h^s h_{32}r_t^s k_t =$$
$$h^s h_{32}r_t^s\left[\begin{array}{c} \left(\dfrac{n\cos(c)+n^2}{(xsin(c))^2}\right)\sin\left(\dfrac{m\pi(x-x_1)}{x_2-x_1}\right) \\ -\dfrac{1}{x}\dfrac{m\pi}{x_2-x_1}\cos\left(\dfrac{m\pi(x-x_1)}{x_2-x_1}\right) \end{array} \right]\cos(nt) \quad (17.d)$$

These equations describe the modal point sensing signals of simply supported conical shells.

6. Validation

In order to validate this methodology, comparisons with the available result in the open literature are made. Modal signals of conical shells with free-free boundary condition was calculated by Tzou et al [5]. In this section model No.1 from [5] is considered to validate the sensor modal voltage calculation procedure. In considered reference, the piezoelectric layer covered the entire conical shell surface and it was segmented into patches. The modal displacement function for free-free boundary condition was considered as [5]:

$$u = \left(\frac{x}{x_2}\right)^m \cos(nt) \quad (18.a)$$

$$v = \left(\frac{x}{x_2}\right)^m \sin(nt) \quad (18.b)$$

$$w = \left(\frac{x}{x_2}\right)^m \cos(nt) \quad (18.c)$$

The Donnel-Mushtari-Vlasov theory was used to develop the strain displacement relation and the in-plane displacements u and v are neglected in the bending strains but not in the membrane strains [5]. By substituting (Eq.18) into (Eq.11) the modal signals of conical shell in the free-free boundary condition can be calculated.

The modal signals of mode (1, 3) are plotted in the Figure.2. Note that the longitudinal bending strain signal vanishes due to the selected displacement function with $m=1$ [5]. Comparing Figure.2 in this study and Figure 5 in [5] it can be concluded that the modal voltage calculation procedure in the conical shell is accurate. To discuss more, the modal signals of mode (2, 5) are calculated and plotted in the Figure.3. The results can be compared with the Figure 11 in [5]. The modal signals are the same and it validates the modal voltage calculation procedure.

(17.a)

(17.b)
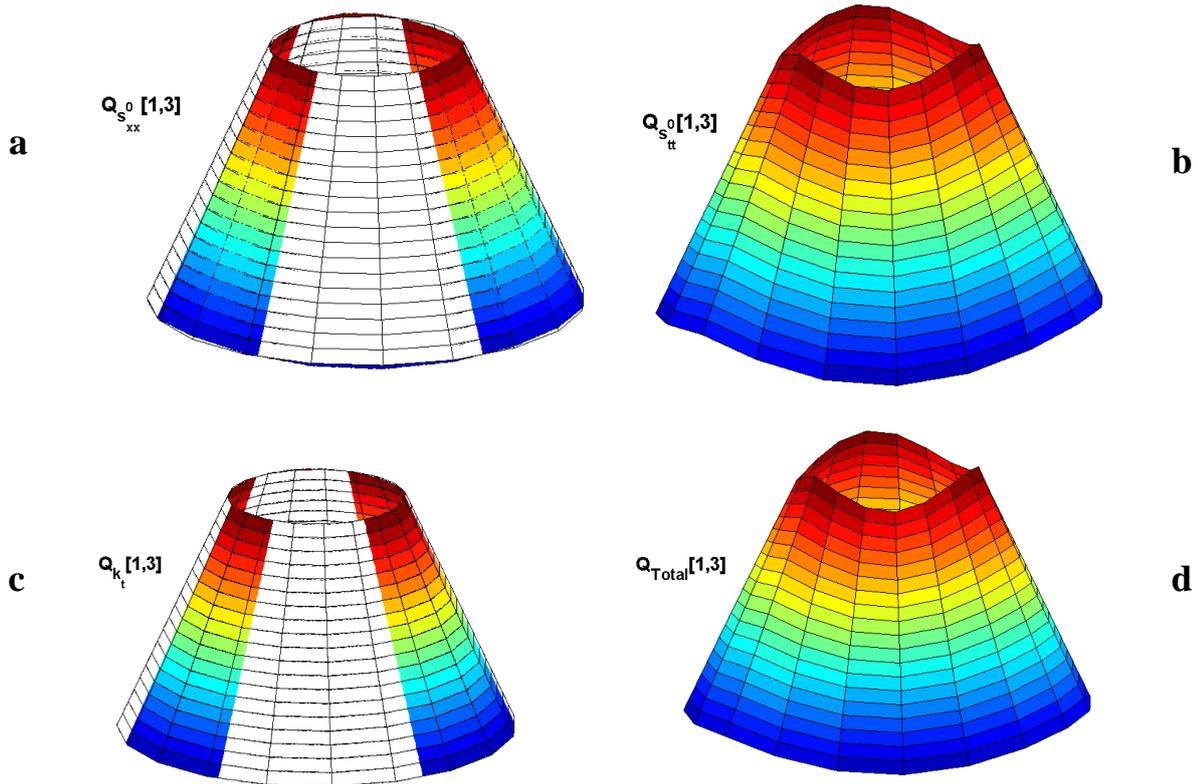
Figure 2: Signal components and modal voltage of (1, 3) mode in free-free boundary condition a) Longitudinal membrane strain signal b) Circumferential membrane strain signal c) Circumferential bending strain signal d) Total strain signal

$Q_{Total}[2,5]$

e
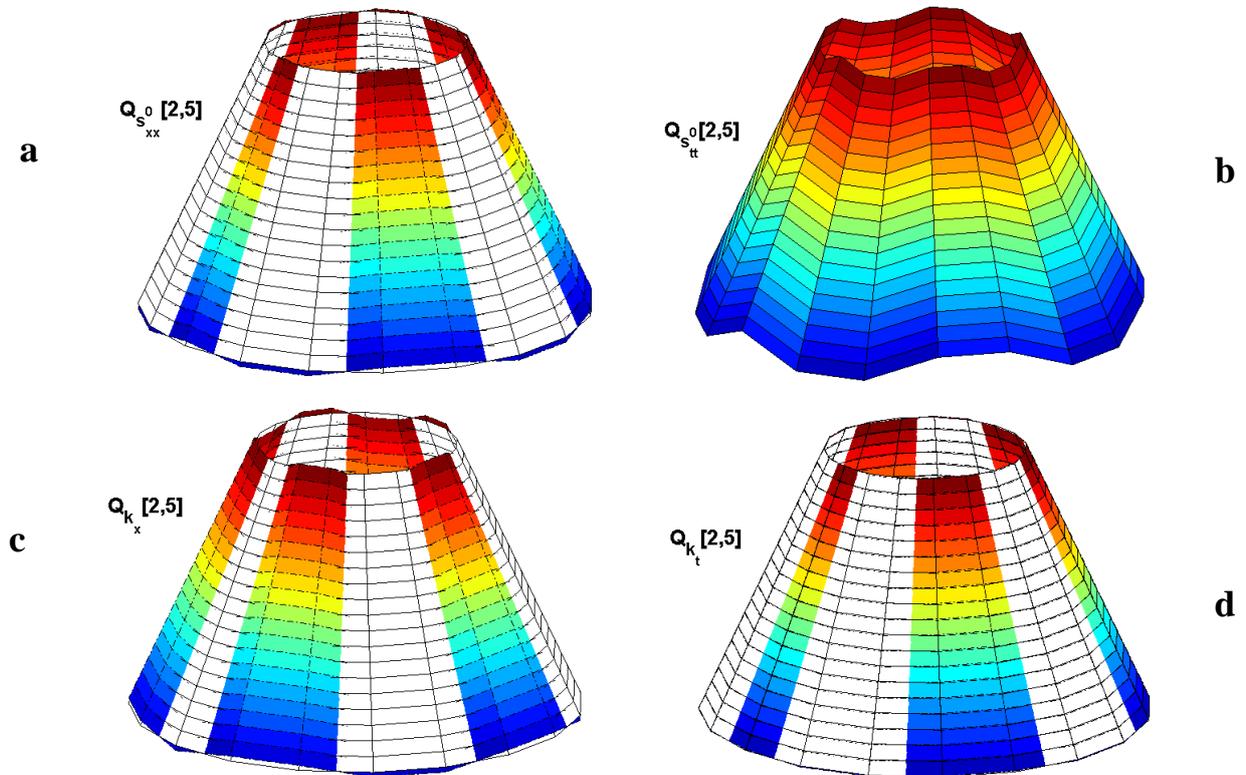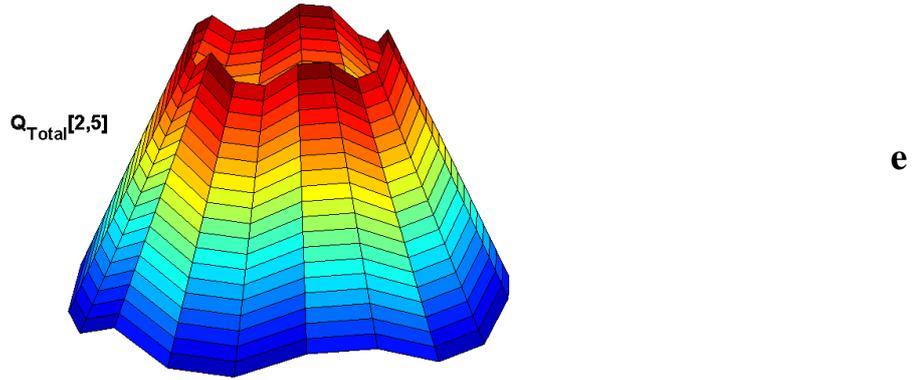
Figure 3: **Signal components and modal voltage of (2, 5) mode in free-free boundary condition a) Longitudinal membrane strain signal b) Circumferential**

7. Case study

In this section a case study is considered to evaluate the transverse sensing of simply supported truncated conical shell. An isotropic conical shell model with simply supported boundary conditions at both ends is considered. The geometric parameters of this model are presented in Table.1. The surface of this model is embedded by piezoelectric layer and this layer is used as sensors. This layer is segmented equally into the 20 parts in the longitudinal and circumferential direction. Therefore, there are 400 sensor patches in the surface of the conical shell and modal voltages of them can be calculated in any mode. (Figure.4)
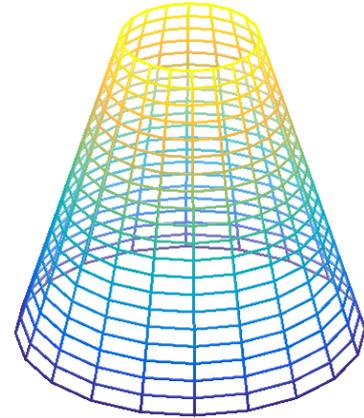
Figure 4. Sensor patches in the conical shell surface.

Table 1. The geometric properties of the model and material properties of the piezoelectric layer

Parameter	Value
x_1	0.2 m
x_2	0.5 m
ψ	$\frac{\pi}{?}$ rad
h^s	0.0005 m
r_x^s	0.0025 m
r_θ^s	0.0025 m
h_{31}	1 V/m
h_{32}	1 V/m

The described modal functions are used as the modal displacement of each conical shell mode. In this investigation, each modal participation factor is assumed to be one. Also, the piezoelectric parameters h_{31}, h_{32} are assumed to be unity. Therefore, by multiplying the sensing signals with the piezoelectric parameters and modal participation factor, the dynamic sensing of the conical shell signals with simply supported boundary conditions can be calculated, simply.

Three groups of mode shapes are considered, namely, $m=1$, $m=2$ and $m=3$ mode group. In each mode group, the longitudinal wave number (m) is constant and different circumferential wave number (n) is considered. In each mode group, three mode shapes with circumferential wave number from 1 to 3 are considered.

In each mode shape, there are six figures, which are shown in the same pattern. The longitudinal membrane and longitudinal bending strains are shown in the top-left and top right plots, respectively. In the middle-left and the middle-right, signal induced by the circumferential membrane strain and the circumferential bending strain are shown, sequentially. In the bottom-left, the sensing signal induced by the overall strain of conical shell is shown. In the bottom-right the considered mode shape displacement is shown. Each mode group is discussed separately and the results of them are shown in separate figures.

7.1. The Mode Group with Longitudinal wave number of 1 (m=1)

Modal signals of the first mode group with longitudinal wave number of 1 ($m=1$) are presented here. The results of mode shapes of ($m=1$, $n=1$), ($m=1$, $n=2$) and ($m=1$, $n=3$) are shown in the Figure.5, Figure.6 and Figure.7, respectively.

In the ($m=1$, $n=1$) mode, the membrane strains signals have a leading role in the total signal and they are dominant in comparison with bending strains signals. In bending signals, the longitudinal bending strain signal has more effect than the

circumferential bending strain signal on the total signal. The longitudinal membrane strain signal and the longitudinal bending strain signal have 180° phase difference and their magnitudes ratio is constant. Considering the Eq.14.a and Eq.14.b and their similarities, this phenomenon is rational and it happens in the entire mode shapes with different constant ratios. In this mode shape, the total signal maximum is located the middle of the major and minor ends ($x = 0.35\text{m}$) and this location is an optimum for sensor patches if the conical shell first mode shape is exited. Usually, high strain regions result in high signal magnitudes.

In the ($m = 1$, $n = 2$) mode, the circumferential membrane signal component is the dominant signal. Afterward, the longitudinal membrane signal component has more effect on the total signal. Bending strain signals of this mode has the least effect on the total signal, specially the circumferential bending signal. The longitudinal membrane strain signal has two maximum which are located in the $x = 0.275\text{m}$ and $x = 0.425\text{m}$ in the longitudinal direction and $t = \pi$ in the circumferential direction, respectively. There are three minimums in this signals which can be localized conveniently. The total signal output has two maximums and two minimums. The minimums are located in the middle of the conical shell surface

in the longitudinal direction ($x = 0.35\text{m}$). In contrast, the maximums are located in the middle of the conical shell surface in the circumferential direction ($t = \pi$).

In the ($m = 1$, $n = 3$) mode, like the previous mode, the circumferential membrane strain signal is dominant in comparison with other signals. Afterward, the order of effectiveness of signals on the total output signal is: the longitudinal membrane strain signal, the circumferential bending strain signal and the longitudinal bending strain signal. In this mode, the maximum of total signal is located at $x = 0.35\text{m}$, in the longitudinal direction and approximately at $t = \frac{2\pi}{3}$, in the circumferential direction. The minimum of total signal is located in the $x = 0.29\text{m}$ in the longitudinal direction and approximately in the $t = \frac{\pi}{3}$ in the circumferential direction. The total signal varies more in the middle of the conical shell in the longitudinal direction and it is almost constant in the major and minor ends of the shell.

Mode Shape Displacement (1,1)

e

f
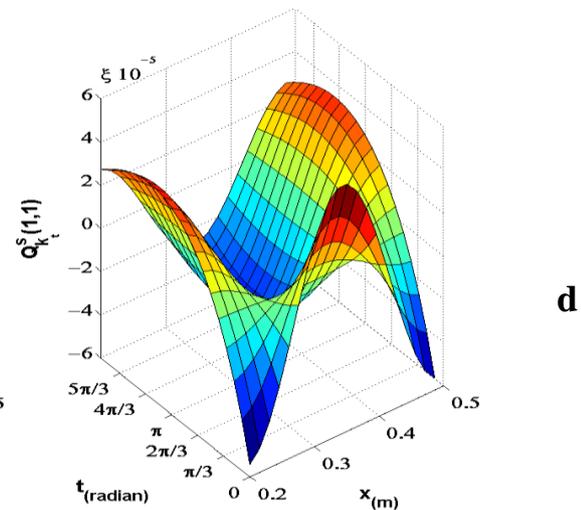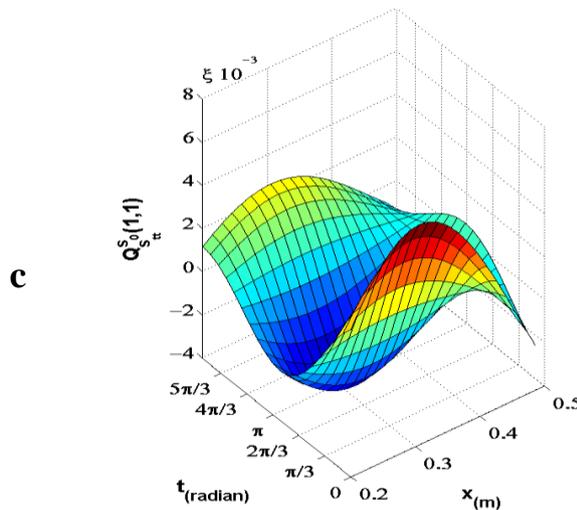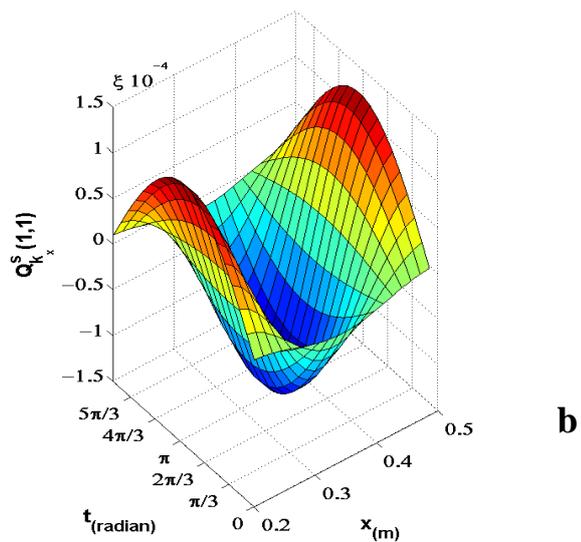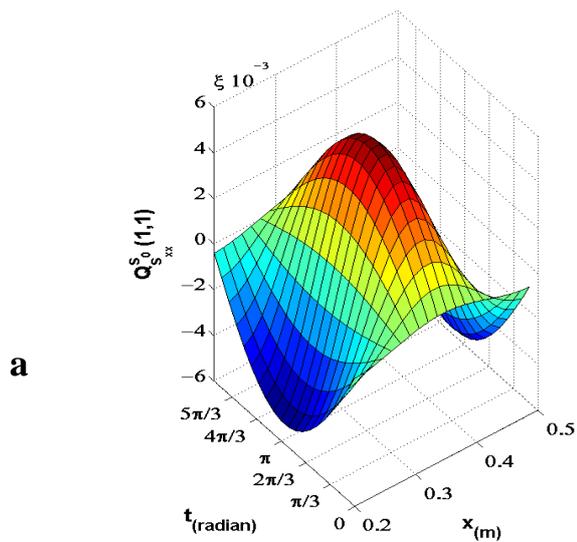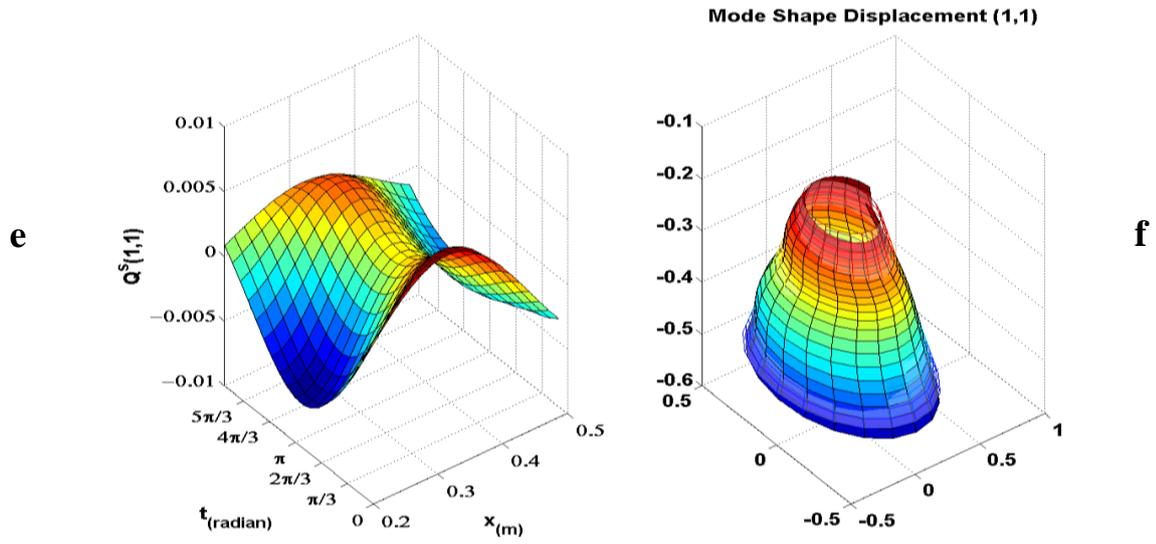
Figure 5: Sensing Signal of Mode (1,1) a) Longitudinal membrane strain signal b) Longitudinal bending strain signal c) Circumferential membrane strain signal d) Circumferential bending strain signal e) Total strain signal f) Mode shape displacement

a

b

c

d
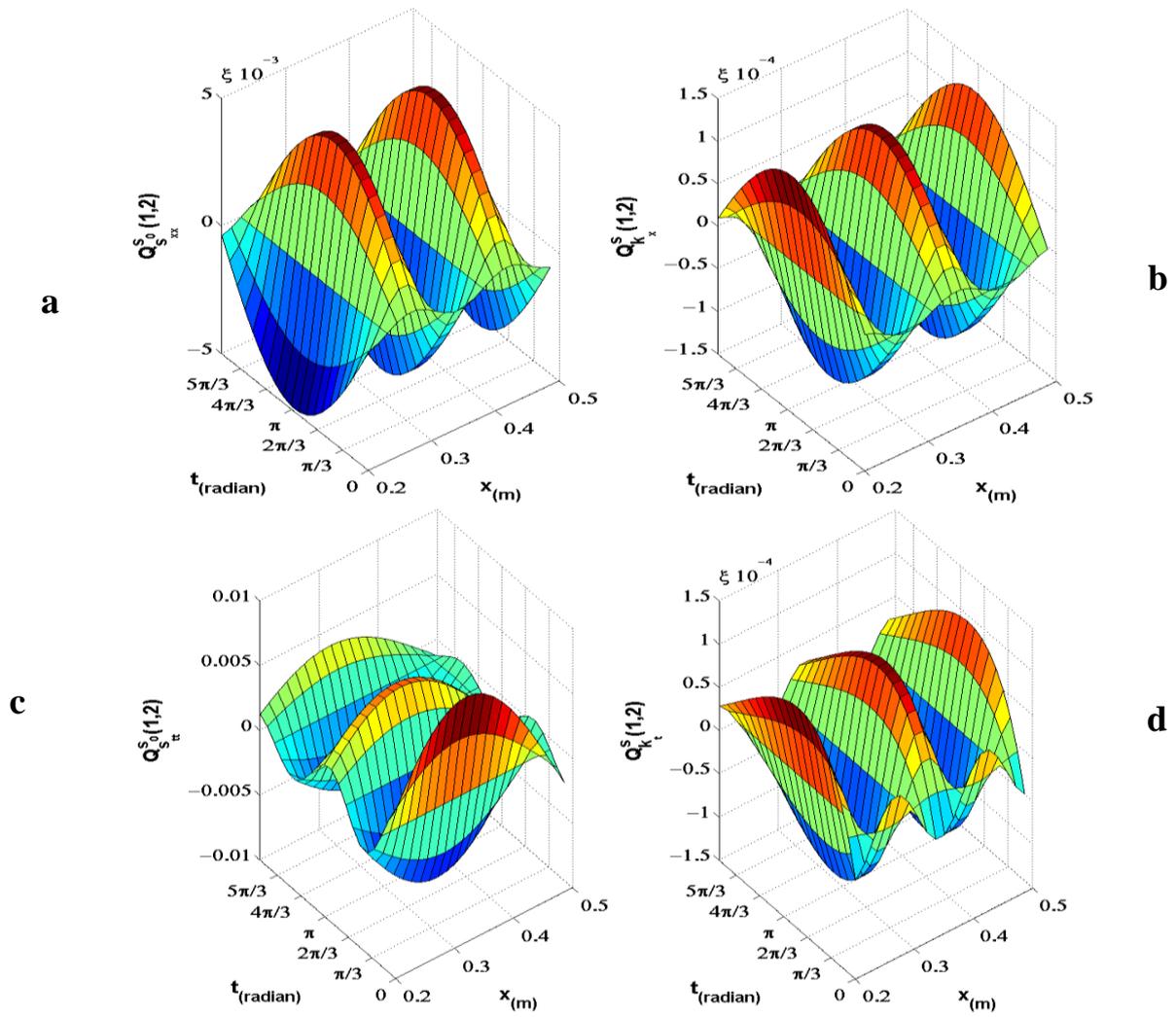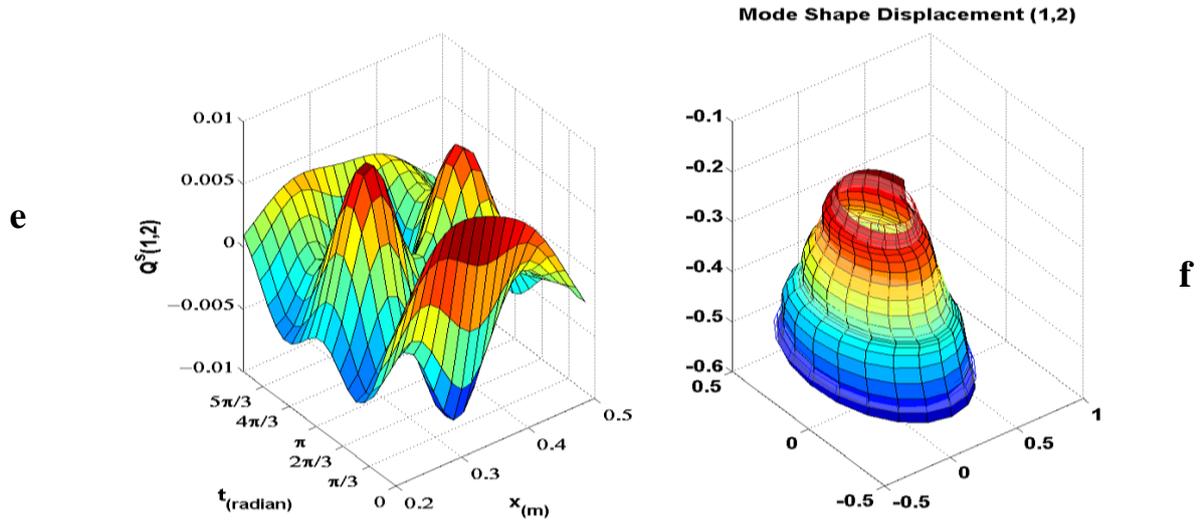
Figure 6: Sensing Signal of Mode (1,2) a) Longitudinal membrane strain signal b) Longitudinal bending strain signal c) Circumferential membrane strain signal d) Circumferential bending strain signal e) Total strain signal f) Mode shape displacement

Mode Shape Displacement (1,3)

e

f
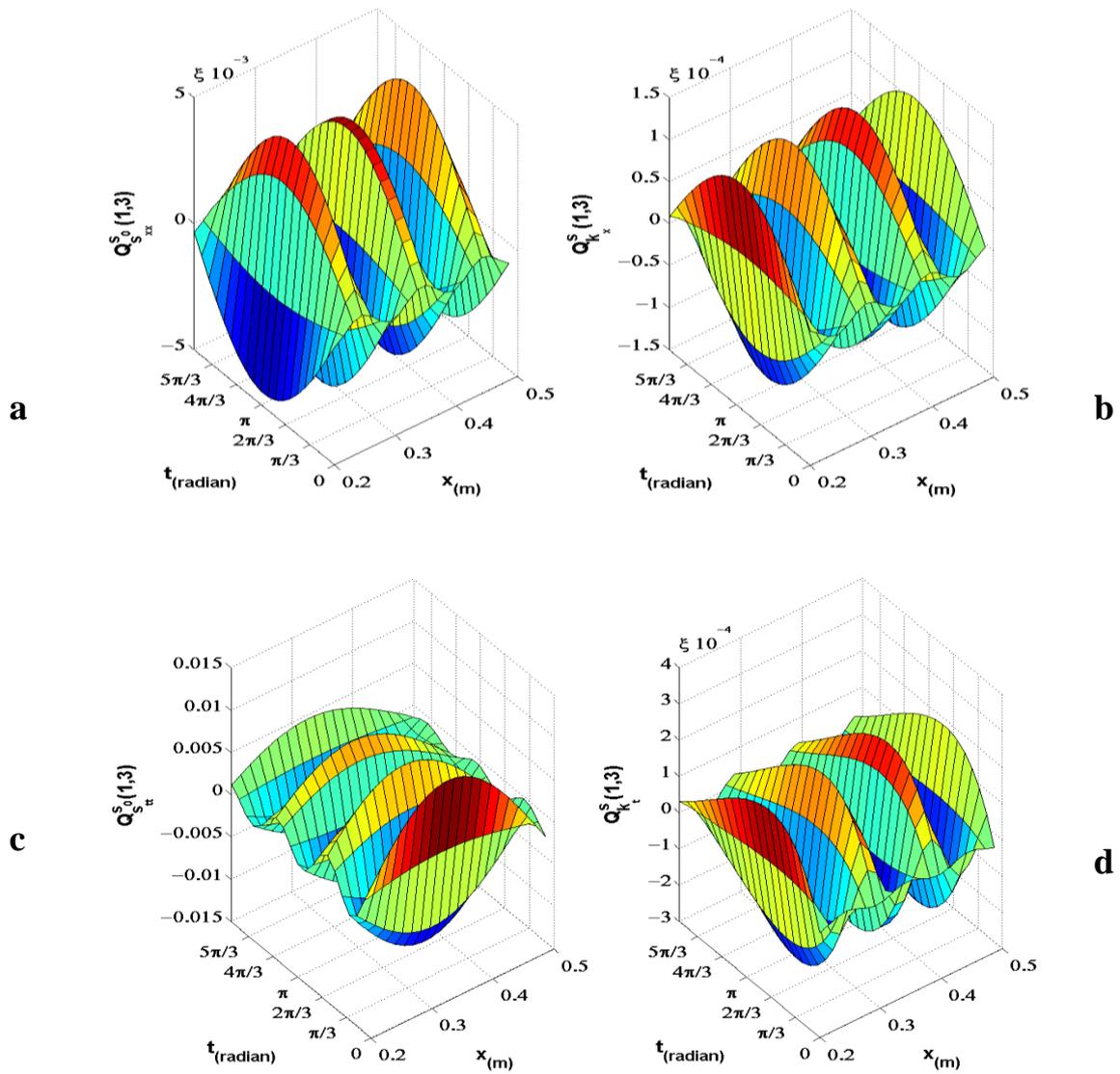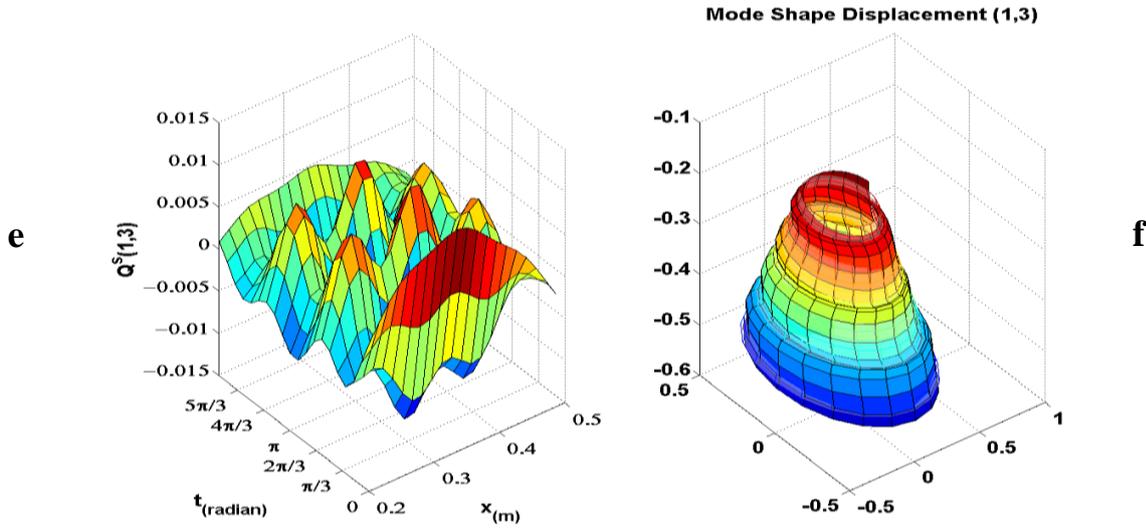
Figure 7: Sensing Signal of Mode (1,3) a) Longitudinal membrane strain signal b) Longitudinal bending strain signal c) Circumferential membrane strain signal d) Circumferential bending strain signal e) Total strain signal f) Mode shape displacement

7.2. The Mode Group with Longitudinal Wave Number of 2 (m=2)

Modal signals and their components in the second mode group ($m = 2$) are presented here. The results of each mode shape ($m = 2, n = 1$), ($m = 2, n = 2$) and ($m = 2, n = 3$) are shown in the Figure.8, Figure.9 and Figure.10, respectively.

In the ($m = 2, n = 1$) mode, the longitudinal membrane strain signal is the most effective one on the total signal and the other signals magnitudes are very low in comparison with this signal. Therefore, the total signal can be estimated as the longitudinal membrane strain signal. The total signal (and consequently the longitudinal membrane strain signal) has three maximums and three minimums, which are located in the major end, in the middle of the shell in the longitudinal direction ($x = 0.45m$) and in the minor end.

In the ($m = 2, n = 2$) mode, the membrane strains signals are more effective than bending strain signals, especially the longitudinal membrane strain signal. The total signal has a maximum which is located at the $x = 0.41m$ and in the $t = \pi/3$, approximately. Similarly, this signal has a minimum which is located at $x = 0.26m$ in the longitudinal direction and in the $t = 3\pi/2$ in the circumferential direction, approximately.

In the ($m = 2, n = 3$) mode like pervious mode, the membrane strains signals are more dominant than that of bending strain signals, and the longitudinal membrane strain is the most dominant signal. The bending strains signals magnitudes are very low in comparison with the membrane strains signals and consequently, the effects of these signals on the total signal are not considerable. The total signal has a maximum and a minimum which are approximately located in the $(0.245m, 2\pi/3)$ and $(0.395m, 2\pi/3)$, respectively. The total signal varies more in the circumferential direction than that of the longitudinal direction.

7.3. The Mode Group with Longitudinal Wave Number of 3 (m=3)

Modal signals for the third mode group with the longitudinal wave number of 3 (m=3) are presented here. The results of each mode shape (m=3, n=1), (m=3, n=2) and (m=3, n=3) are shown in the Figure.11, Figure.12 and Figure.13, respectively.

In the (m=3, n=1) mode, the longitudinal membrane strain signal has the most influence on the total signal and the other signals magnitudes are very low in comparison with this signal. Therefore, the total output signal can be estimated as the same as the longitudinal membrane strain signal. The total output signal (and consequently the longitudinal membrane strain signal) has four maximums and five minimums which are located in the major end, in the middle of the conical shell in the longitudinal direction and in the minor end. The total signal variations in both directions are high and in major and minor ends, the signal variation increases.

In the (m=3, n=2) mode, the membrane strain signals are more dominant than bending strain signals, specially the longitudinal membrane strain signal. The total output signal has six maximums, which two of them are located in the middle of the shell surface and four of them are located in the minor and major ends of the conical shell. Similarly, the total output signal has six minimums, which two of them are located in the middle of the longitudinal direction of the shell surface and four of them are located in the minor and major ends of the conical shell.

In the (m=3, n=3) mode, the membrane strain signals are more dominant than bending strain signals, and the longitudinal membrane signal has more effect on the total output signal in comparison with the circumferential membrane strain signal. The total output signal has two maximums which are approximately located in the middle of the conical shell in the longitudinal direction (x=0.35 m). Similarly, the total output signal has two minimums which are approximately located in the middle of the conical shell in the circumferential direction (t=π).
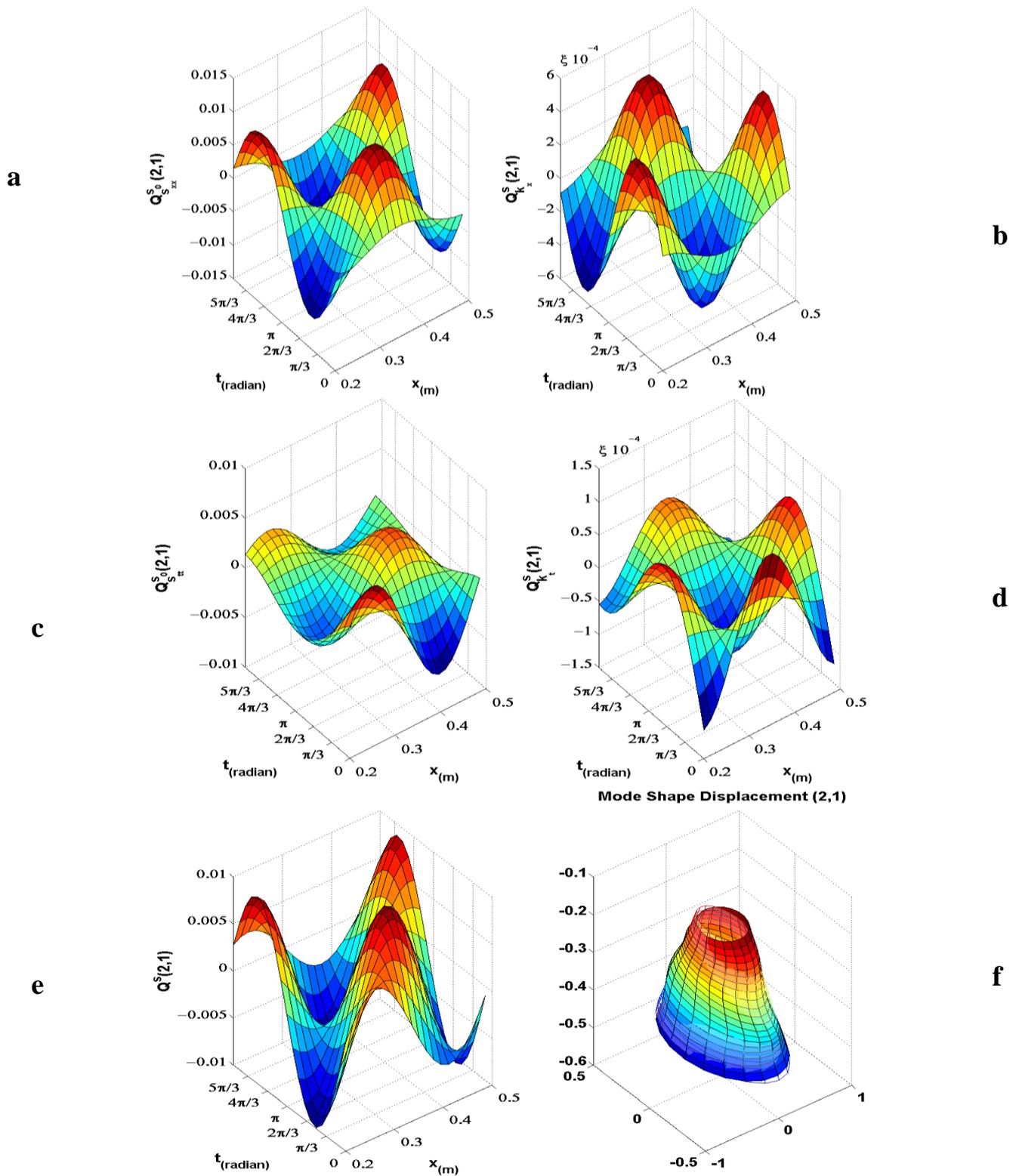
Figure 8: Sensing Signal of Mode (2,1) a) Longitudinal membrane strain signal b) Longitudinal bending strain signal c) Circumferential membrane strain signal d) Circumferential bending strain signal e) Total strain signal f) Mode shape displacement
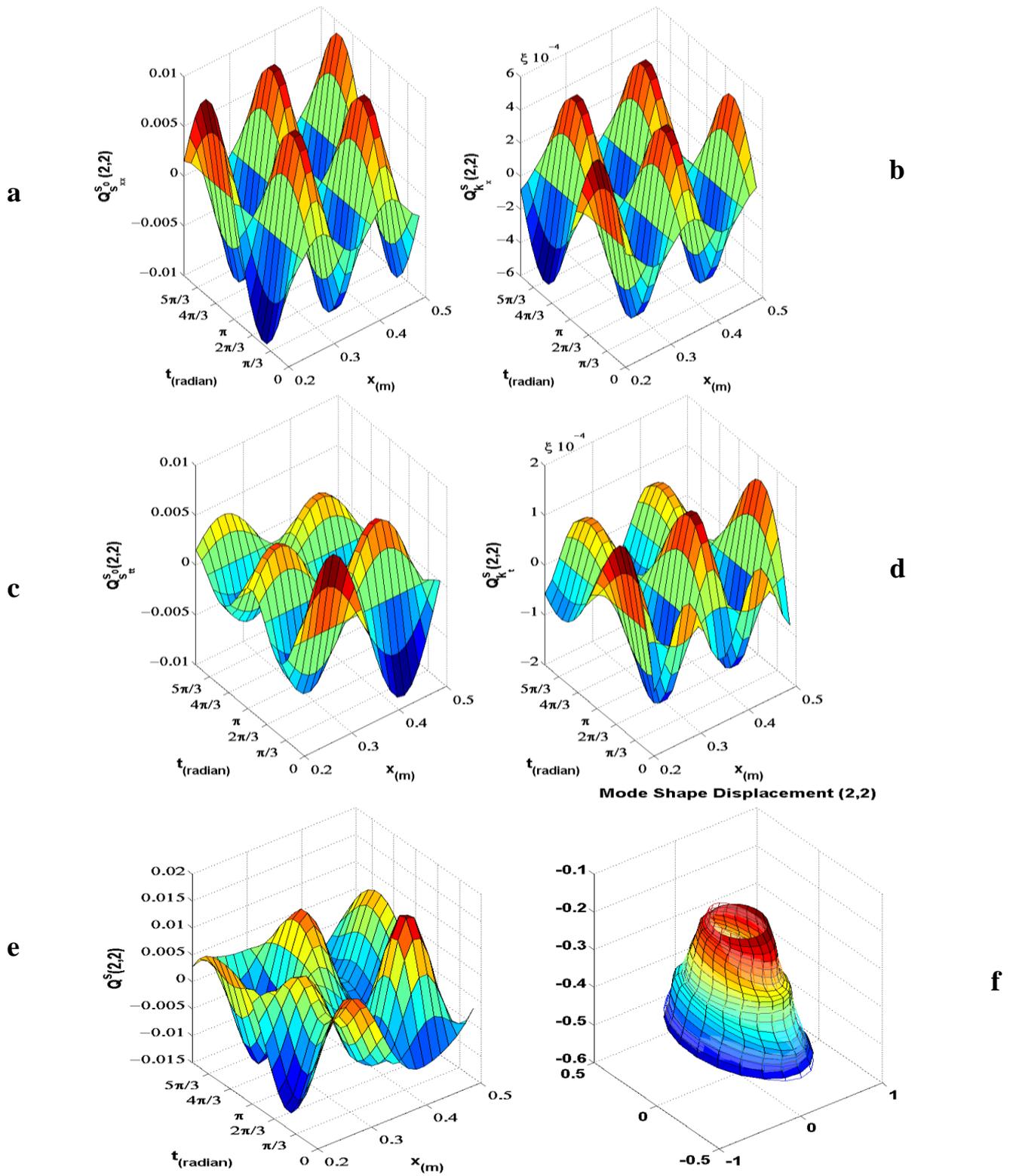
Figure 9: Sensing Signal of Mode (2,2) a) Longitudinal membrane strain signal b) Longitudinal bending strain signal c) Circumferential membrane strain signal d) Circumferential bending strain signal e) Total strain signal f) Mode shape displacement
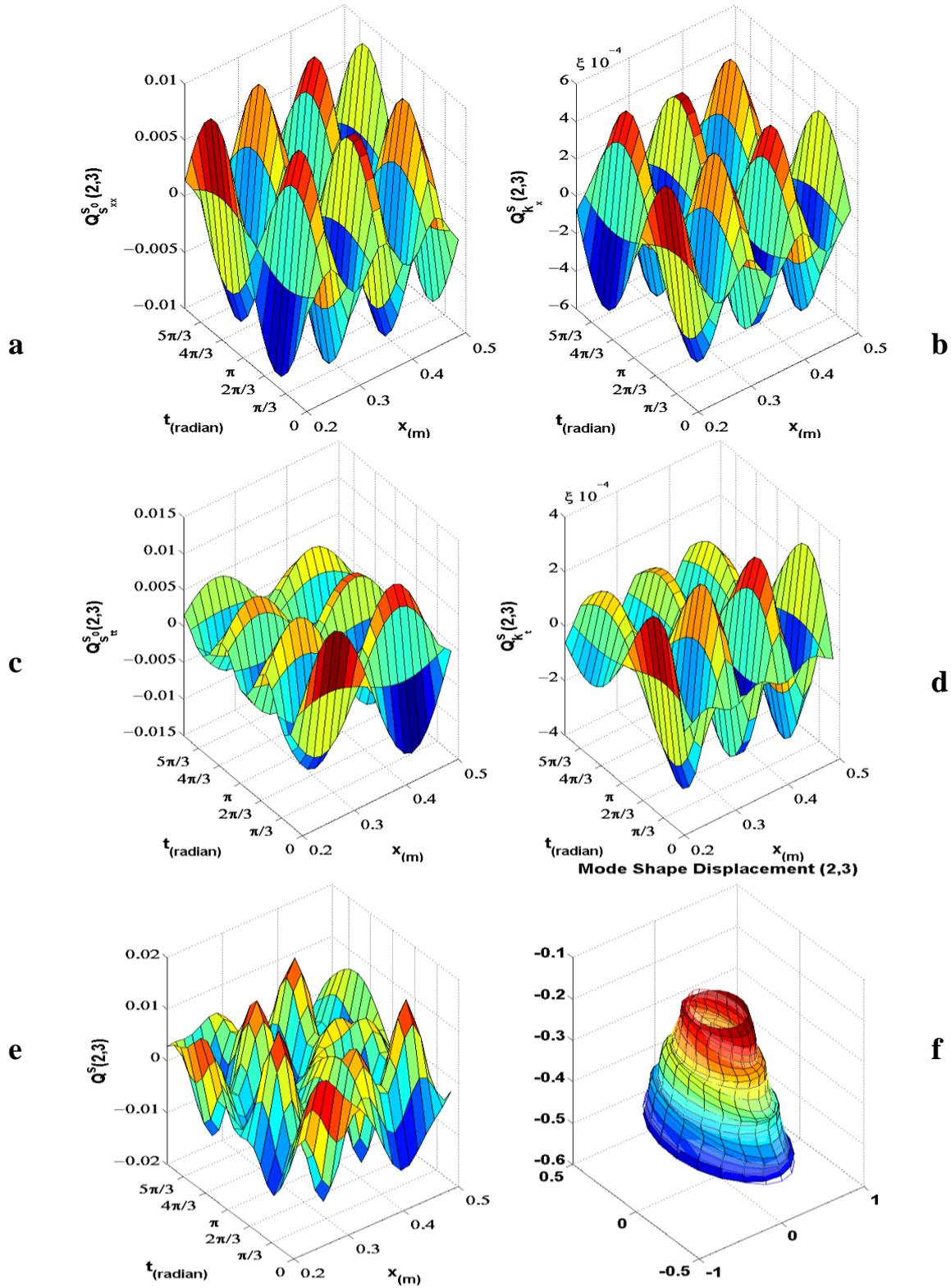
Figure 10: Sensing Signal of Mode (2,3) a) Longitudinal membrane strain signal b) Longitudinal bending strain signal c) Circumferential membrane strain signal d) Circumferential bending strain signal e) Total strain signal f) Mode shape displacement
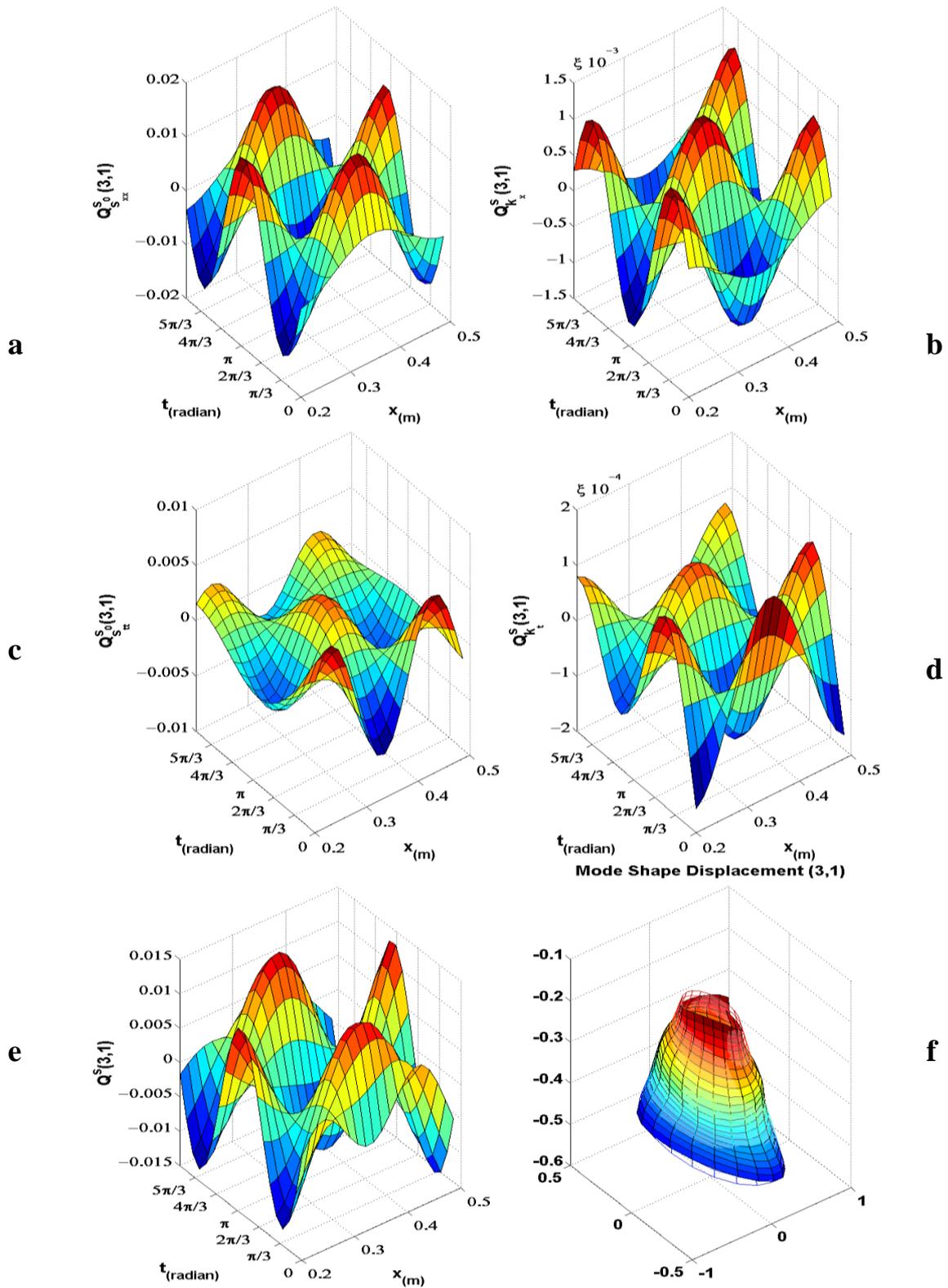
Figure 11: Sensing Signal of Mode (3,1) a) Longitudinal membrane strain signal b) Longitudinal bending strain signal c) Circumferential membrane strain signal d) Circumferential bending strain signal e) Total strain signal f) Mode shape displacement
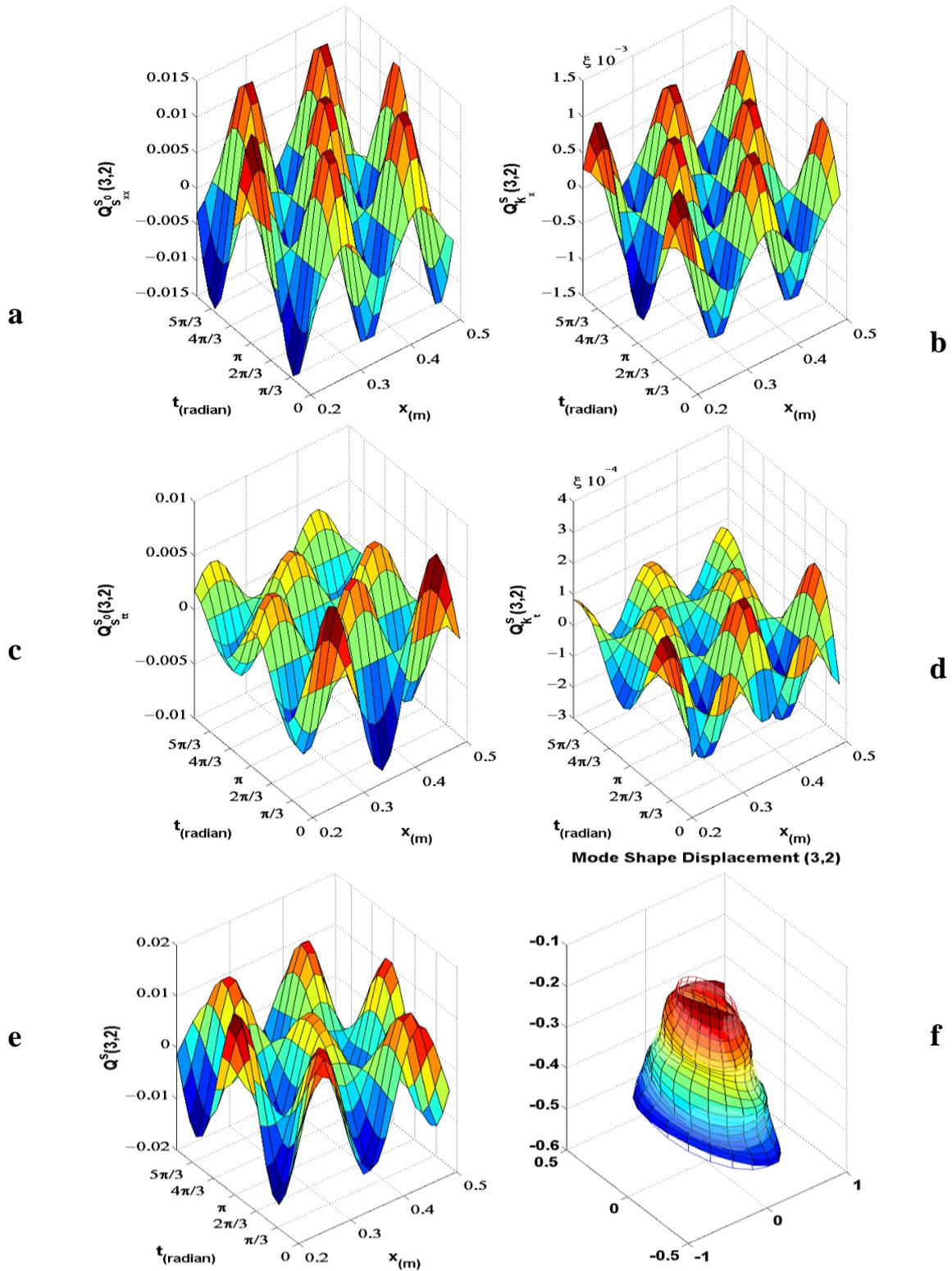
Figure 12: Sensing Signal of Mode (3,2) a) Longitudinal membrane strain signal b) Longitudinal bending strain signal c) Circumferential membrane strain signal d) Circumferential bending strain signal e) Total strain signal f) Mode shape displacement
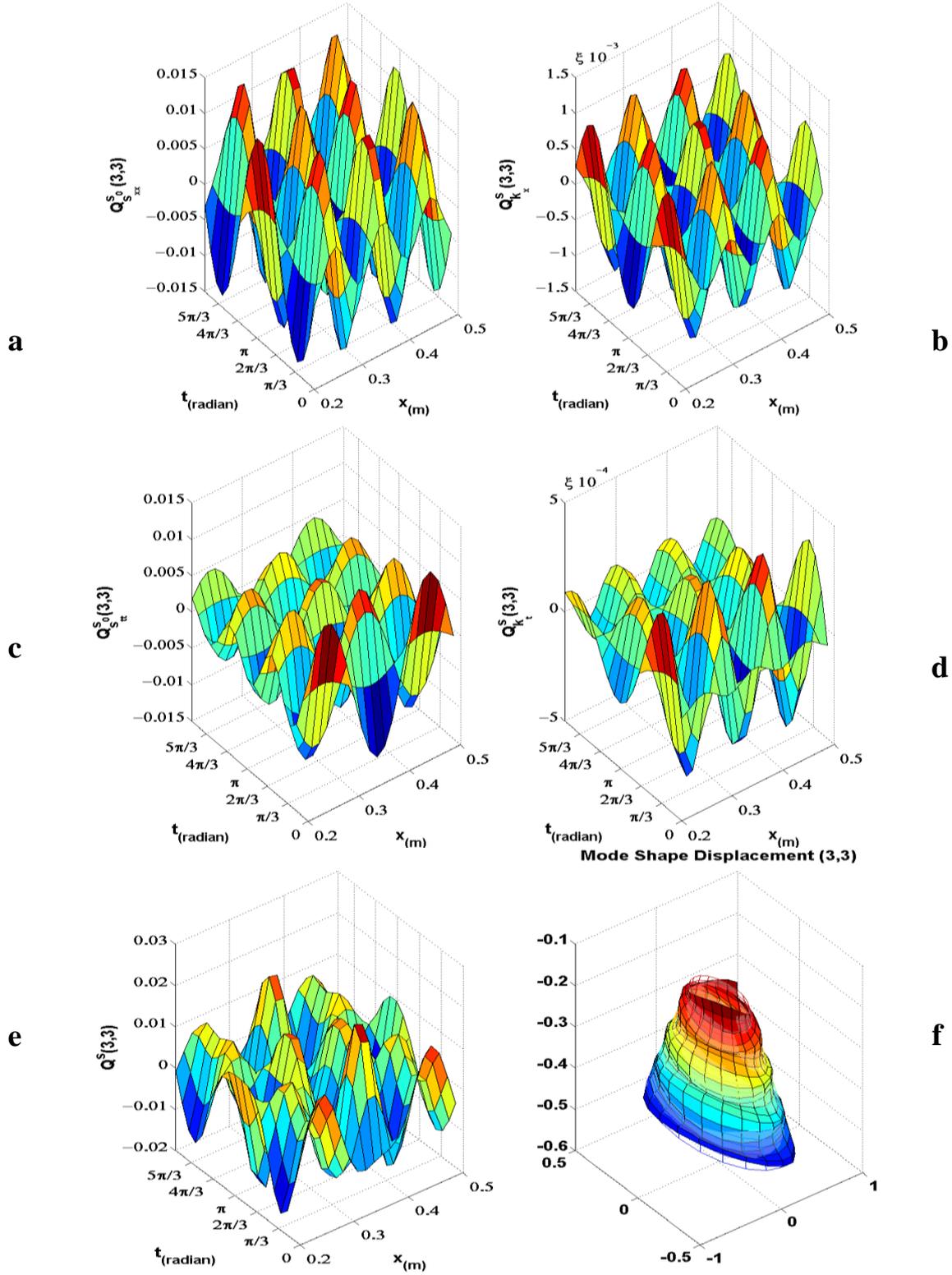
Figure 13: Sensing Signal of Mode (3,3) a) Longitudinal membrane strain signal b) Longitudinal bending strain signal c) Circumferential membrane strain signal d) Circumferential bending strain signal e) Total strain signal f) Mode shape displacement

The distributed signal patterns clearly represent the modal dynamic and strain characteristics of conical shells in simply supported boundary condition. These results propose the ideal sensor locations in considered mode shapes. The location of sensor should be chosen at a place where maximum displacement happens and a controller should be designed to suspend this vibration. If one mode shape is excited, the sensor should be located at the region where the amplitude of the total signal in considered mode shape is optimal. On the other hand, if a mode shape is not excited and aimed to be avoided, the sensor must be

located in the regions with zero total output signal in considered mode shape. Therefore, in overall to control the vibration of simply supported conical shell, first it should be defined which modes is excited and ideal location for sensor patches should be identified from the aforementioned results. By this method, conical shell vibration can be observed and controlled consequently. Distributed signals also reveal critical regions showing significant or minimal signal magnitudes.

Appropriate selection of regional signal components can further enhance the distributed control effectiveness of conical shells. In simply supported conical shell the membrane signals are more effective than the bending signals. The bending signals can be neglected almost in all of mode shapes. In the mode group with longitudinal wave number of 1, the circumferential membrane strain signal is the dominant signal and in other modes, the longitudinal membrane strain signal is the dominant signal. Therefore, it can be concluded that the longitudinal membrane strain signal in the simply supported conical shell is the most dominant signal among the other signals. The reason of this phenomenon is the strain displacement relation in the conical shells and the simply supported boundary condition mode shapes.

In the considered case study, all of the shell area was embedded by piezoelectric layer. There is no rule to cover the entire shell surface with piezoelectric sensors, considering the price of the piezoelectric layer, a strip of sensor is more desirable than the entire shell surface covered with piezoelectric sensors. So, the sensor can be a strip which is distributed in the surface of the conical shell longitudinally, circumferentially.

8. Conclusions

The transverse sensing of simply supported conical shell with piezoelectric layer was studied in the present paper. Governing sensing signal displacement equations were derived based on the Kirchhoff theory, thin-shell assumption, piezoelectric direct effect, the Gauss theory and the open circuit assumption. The total modal signal consists of four components resulting from the four strain components. In the first mode group the circumferential membrane strain signal is the dominant signal and after that the longitudinal membrane strain signal has the most effect on the total output of sensor. While, in other mode groups, the longitudinal membrane strain signal is more dominant than others. Consequently, it can be concluded that in the simply supported conical shell, the longitudinal membrane strain signal has a leading role in the total sensor output. The ideal locations of the piezoelectric sensor for sensing the transverse vibration of simply supported truncated conical shell were identified in considered modes. The output signals of the sensor can be used as the control input for later active vibration control or it can be used for structural health monitoring.

References

[1]   D. Thakkar, R. Ganguli, Induced shear actuation of helicopter rotor blade for active twist control, *Thin-Walled Structures,* Vol. 45, No. 1, pp. 111-121, 2007/01/01/, 2007.

[2]   F.-M. Li, K. Kishimoto, W.-H. Huang, The calculations of natural frequencies and forced vibration responses of conical shell using the Rayleigh–Ritz method, *Mechanics Research Communications,* Vol. 36, No. 5, pp. 595-602, 2009/07/01/, 2009.

[3]   K. Y. Lam, L. Hua, Vibration analysis of a rotating truncated circular conical shell, *International Journal of Solids and Structures,* Vol. 34, No. 17, pp. 2183-2197, 1997/06/01/, 1997.

[4]   H. Li, Z. B. Chen, H. S. Tzou, Torsion and transverse sensing of conical shells, *Mechanical Systems and Signal Processing,* Vol. 24, No. 7, pp. 2235-2249, 2010/10/01/, 2010.

[5]   H. S. Tzou, W. K. Chai, D. W. Wang, Modal voltages and micro-signal analysis of conical shells of revolution, *Journal of Sound and Vibration,* Vol. 260, No. 4, pp. 589-609, 2003/02/27/, 2003.

[6]   W. K. Chai, P. Smithmaitrie, H. S. Tzou, Neural potentials and micro-signals of non-linear deep and shallow conical shells, *Mechanical Systems and Signal Processing,* Vol. 18, No. 4, pp. 959-975, 2004/07/01/, 2004.

[7]   F.-M. Li, Z.-G. Song, Z.-B. Chen, Active vibration control of conical shells using piezoelectric materials, *Journal of Vibration and Control,* Vol. 18, No. 14, pp. 2234-2256, 2012/12/01, 2011.

[8]   M. Safarabadi, M. Mohammadi, A. Farajpour, M. Goodarzi, Effect of surface energy on the vibration analysis of rotating nanobeam, *Journal of Solid Mechanics,* Vol. 7, No. 3, pp. 299-311, 2015.

[9]   M. Mohammadi, M. Safarabadi, A. Rastgoo, A. Farajpour, Hygro-mechanical vibration analysis of a rotating viscoelastic nanobeam embedded in a visco-Pasternak elastic medium and in a nonlinear thermal environment, *Acta Mechanica,* Vol. 227, No. 8, pp. 2207-2232, 2016.

[10]   M. Danesh, A. Farajpour, M. Mohammadi, Axial vibration analysis of a tapered nanorod based on nonlocal elasticity theory and differential quadrature method, *Mechanics Research Communications,* Vol. 39, No. 1, pp. 23-27, 1//, 2012.

[11]   M. Goodarzi, M. Mohammadi, M. Khooran, F. Saadi, Thermo-Mechanical Vibration Analysis of FG Circular and Annular Nanoplate Based on the Visco-Pasternak Foundation, *Journal of Solid Mechanics,* Vol. 8, No. 4, pp. 788-805, 2016.

[12]   M. Mohammadi, M. Ghayour, A. Farajpour, Analysis of free vibration sector plate based on elastic medium by using new version of differential quadrature method, 2011.

[13]   M. Goodarzi, M. Mohammadi, A. Farajpour, M. Khooran, Investigation of the Effect of Pre-Stressed on Vibration Frequency of Rectangular Nanoplate Based on a Visco-Pasternak Foundation, *Journal of Solid Mechanics,* Vol. 6, No. 1, pp. 98-121, 2014.

[14]   M. R. Farajpour, A. Rastgoo, A. Farajpour, M. Mohammadi, Vibration of piezoelectric nanofilm-based electromechanical sensors via higher-order non-local strain gradient theory, *Micro & Nano Letters,* 11, 2016.

[15]   M. Mohammadi, M. Goodarzi, M. Ghayour, S. Alivand, Small scale effect on the vibration of orthotropic plates embedded in an elastic medium and under biaxial in-plane pre-load via nonlocal elasticity theory, *Journal of Solid Mechanics,* Vol. 4, No. 2, pp. 128-143, 2012.

[16]   H. Asemi, S. Asemi, A. Farajpour, M. Mohammadi, Nanoscale mass detection based on vibrating piezoelectric ultrathin films under thermo-electro-mechanical loads, *Physica E: Low-dimensional Systems and Nanostructures,* Vol. 68, pp. 112-122, 2015.

[17]   M. Mohammadi, A. Farajpour, M. Goodarzi, H. Mohammadi, Temperature effect on vibration analysis of annular graphene sheet embedded on visco-pasternak foundation, *J. Solid Mech,* Vol. 5, pp. 305-323, 2013.

[18]   M. Mohammadi, A. Farajpour, M. Goodarzi, R. Heydarshenas, Levy type solution for nonlocal thermo-mechanical vibration of orthotropic mono-layer graphene sheet embedded in an elastic medium, *Journal of Solid Mechanics,* Vol. 5, No. 2, pp. 116-132, 2013.

[19]   M. Mohammadi, A. Moradi, M. Ghayour, A. Farajpour, Exact solution for thermo-mechanical vibration of

orthotropic mono-layer graphene sheet embedded in an elastic medium, *Latin American Journal of Solids and Structures,* Vol. 11, No. 3, pp. 437-458, 2014.

[20] M. Mohammadi, A. Farajpour, M. Goodarzi, F. Dinari, Thermo-mechanical vibration analysis of annular and circular graphene sheet embedded in an elastic medium, *Latin American Journal of Solids and Structures,* Vol. 11, No. 4, pp. 659-682, 2014.

[21] M. Mohammadi, A. Farajpour, M. Goodarzi, Numerical study of the effect of shear in-plane load on the vibration analysis of graphene sheet embedded in an elastic medium, *Computational Materials Science,* Vol. 82, pp. 510-520, 2014.

[22] M. Mohammadi, M. Ghayour, A. Farajpour, Free transverse vibration analysis of circular and annular graphene sheets with various boundary conditions using the nonlocal continuum plate model, *Composites Part B: Engineering,* Vol. 45, No. 1, pp. 32-42, 2013.

[23] M. Mohammadi, M. Goodarzi, M. Ghayour, A. Farajpour, Influence of in-plane pre-load on the vibration frequency of circular graphene sheet via nonlocal continuum theory, *Composites Part B: Engineering,* Vol. 51, pp. 121-129, 2013.

[24] M. Mohammadi, A. Farajpour, A. Moradi, M. Ghayour, Shear buckling of orthotropic rectangular graphene sheet embedded in an elastic medium in thermal environment, *Composites Part B: Engineering,* Vol. 56, pp. 629-637, 2014.

[25] A. Farajpour, M. Mohammadi, A. Shahidi, M. Mahzoon, Axisymmetric buckling of the circular graphene sheets with the nonlocal continuum plate model, *Physica E: Low-dimensional Systems and Nanostructures,* Vol. 43, No. 10, pp. 1820-1825, 2011.

[26] S. Asemi, A. Farajpour, H. Asemi, M. Mohammadi, Influence of initial stress on the vibration of double-piezoelectric-nanoplate systems with various boundary conditions using DQM, *Physica E: Low-dimensional Systems and Nanostructures,* Vol. 63, pp. 169-179, 2014.

[27] A. Farajpour, M. H. Yazdi, A. Rastgoo, M. Loghmani, M. Mohammadi, Nonlocal nonlinear plate model for large amplitude vibration of magneto-electro-elastic nanoplates, *Composite Structures,* Vol. 140, pp. 323-336, 2016.

[28] S. R. Asemi, M. Mohammadi, A. Farajpour, A study on the nonlinear stability of orthotropic single-layered graphene sheet based on nonlocal elasticity theory, *Latin American Journal of Solids and Structures,* Vol. 11, No. 9, pp. 1515-1540, 2014.

[29] A. Farajpour, A. Rastgoo, M. Mohammadi, Vibration, buckling and smart control of microtubules using piezoelectric nanoshells under electric voltage in thermal environment, *Physica B: Condensed Matter,* Vol. 509, pp. 100-114, 2017.

[30] A. Farajpour, A. Rastgoo, M. Mohammadi, Surface effects on the mechanical characteristics of microtubule networks in living cells, *Mechanics Research Communications,* Vol. 57, pp. 18-26, 2014/04/01/, 2014.

[31] S. Asemi, A. Farajpour, M. Mohammadi, Nonlinear vibration analysis of piezoelectric nanoelectromechanical resonators based on nonlocal elasticity theory, *Composite Structures,* Vol. 116, pp. 703-712, 2014.

[32] H. Moosavi, M. Mohammadi, A. Farajpour, S. Shahidi, Vibration analysis of nanorings using nonlocal continuum mechanics and shear deformable ring theory, *Physica E: Low-dimensional Systems and Nanostructures,* Vol. 44, No. 1, pp. 135-140, 2011.